

Electrochemistry

Layered Post-Transition-Metal Dichalcogenides (X–M–M–X) and Their Properties

Jan Luxa⁺,^[a] Yong Wang⁺,^[b] Zdenek Sofer,^[a] and Martin Pumera^{*[b]}

Abstract: A^{III}B^{VI} chalcogenides are an interesting group of layered semiconductors with several attractive properties, such as tunable band gaps and the formation of solid solutions. Unlike the typically sandwiched structure of transition-metal dichalcogenides, A^{III}B^{VI} layered chalcogenides with hexagonal symmetry are stacked through the X–M–M–X motif, in which M is gallium and indium, and X is sulfur, selenium, and tellurium. In view of the inadequate study of the electrochemical properties and great interest in layered ma-

terials towards energy-related research, herein the inherent electrochemistry of GaS, GaSe, GaTe, and InSe has been studied, as well as the exploration of their potential as hydrogen evolution reaction (HER) electrocatalysts. All four materials show redox peaks during cyclic voltammetry measurements. Furthermore, insights into catalysis of the HER are provided; these indicate the conductivity and number of active sites of the materials. All of these findings have important implications on their possible applications.

Introduction

Layered transition-metal dichalcogenides (TMDs) have been attracting great interest due to the unusual properties they exhibit when exfoliated down to mono- or few-layered material.^[1–6] In addition to TMDs, there is a family of A^{III}B^{VI} layered chalcogenides that also exhibit a layered two-dimensional structure, which gives rise to intriguing properties. The compounds are semiconductors with band gap energies that go from the UV region up to the near-infrared (NIR) region. GaS has a band gap energy of 3.05 eV, whereas InSe has a band gap energy of 1.25 eV. These compounds have the general formula of MX, in which M represents gallium and indium and X stands for sulfur, selenium, and tellurium. Compounds with M₂X₃ stoichiometry and the same composition also exist, but do not generally exhibit layered structures.^[7,8] Unlike TMDs, in which one metal and two chalcogen atoms form one layer, A^{III}B^{VI} semiconductors have layers composed of two metal and two chalcogen atoms, giving rise to a X–M–M–X motif. The exception is GaTe, in which the presence of a large anion leads to a reduction in symmetry from hexagonal to monoclinic. Similar to the case of TMDs, these motifs are stacked by weak

van der Waals forces to create three-dimensional structures.^[9–12]

Numerous publications concerning the potential applications of these compounds have been published. For example, gallium sulfide coupled with carbon nanotubes can be used as a high-performance anode in a lithium-ion battery.^[13] GaS also allowed for the construction of highly responsive photodetectors on both rigid and flexible substrates.^[14–16] The preparation of promising electrocatalysts for the hydrogen evolution reaction (HER) from GaS has also been demonstrated.^[11] Last, but not least, the construction of ultrathin GaS transistors has also been demonstrated.^[17] Similarly, GaSe was studied quite extensively. Numerous papers concern its use as a transistor,^[17] photodetector,^[18] part of nonlinear optics,^[19] terahertz radiation source,^[20] and many more applications. The catalytic properties of GaSe have also been studied previously.^[21]

Unlike gallium sulfide and selenide, gallium telluride remains relatively unexplored. Most reports are on the synthesis^[22,23] or optical properties,^[23,24] with no reports on the electrochemistry or catalytic properties of GaTe. Similarly, the investigation of indium selenide remains limited to applications in electronics, such as high-mobility field-effect transistors (FETs)^[25,26] and optoelectronics as image sensors.^[27]

Although a number of papers have studied the properties of A^{III}B^{VI} layered chalcogenides and their possible applications, there is a lack of comparative study of the properties of IIIA group chalcogenides, namely, GaS, GaSe, GaTe, and InSe, from the viewpoint of electrocatalysis. Upon considering promising results of gallium sulfide towards the HER,^[11] it is of high importance to explore the HER performance of A^{III}B^{VI} layered chalcogenides in more detail. Therefore, herein we fundamentally explore the electrochemical properties of A^{III}B^{VI} layered chalcogenides and their HER catalytic performances.

[a] Dr. J. Luxa,⁺ Prof. Z. Sofer
Department of Inorganic Chemistry
University of Chemistry and Technology Prague
Technická 5, 166 28 Prague 6 (Czech Republic)

[b] Y. Wang,⁺ Prof. M. Pumera
Division of Chemistry and Biological Chemistry
School of Physical and Mathematical Science
Nanyang Technological University, 21 Nanyang Link, 637371 (Singapore)
E-mail: Pumera@ntu.edu.sg

[†] These authors contributed equally to this work.

Supporting information for this article is available on the WWW under <http://dx.doi.org/10.1002/chem.201604168>.

Results and Discussion

Herein, we investigated the electrochemical properties of $A^{III}B^{VI}$ layered chalcogenides, namely, GaS, GaSe, GaTe, and InSe. The structure of these compounds is displayed in Figure 1, showing the X–M–M–X arrangement, which can be seen for the hexagonal structure of GaS and InSe with $P6_3/mmc$ symmetry and GaSe with $\bar{P}6m2$ symmetry. The differences in point group only originate from different stacking methods of individual layers. GaTe has significantly lower symmetry, with a monoclinic structure (space group $B2m$). Optical images of the corresponding synthesized samples are shown in Figure 1 together with the structures.

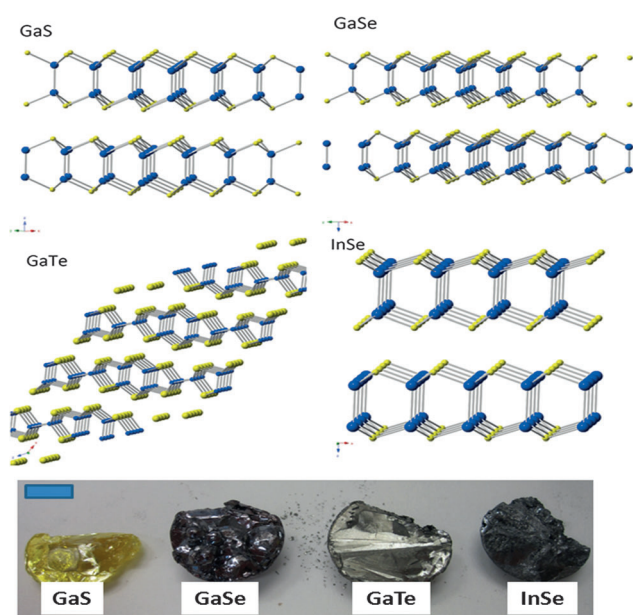


Figure 1. Structures of GaS, GaSe, GaTe, and InSe. Blue dots correspond to the metal and yellow dot corresponds to the chalcogen. Optical images of the corresponding synthesized materials are also shown. Scale bar: 1 cm.

The surface morphology of prepared $A^{III}B^{VI}$ layered chalcogenides was examined by means of SEM. Figure 2 presents the scanning electron micrographs of GaS, GaSe, GaTe, and InSe. The layered structure with no clear delamination, as expected for bulk material, is clearly observed. Furthermore, we performed energy-dispersive X-ray spectroscopy (EDS) to analyze the elemental composition. Results in Figure S1 and Table S1 in the Supporting Information showcase the homogeneous distribution of elements together with the chalcogen to metal ratio close to one, which indicates the successful synthesis of bulk GaS, GaSe, GaTe, and InSe.

More information about the base and edge plane morphology was acquired through AFM measurements (Figure S2 in the Supporting Information). Base planes with steps varying from several nanometers to several hundred nanometers are clearly observable in the base plane figures. The edge plane measurements revealed a much more random distribution of individual sheets. This distribution is attributed to the damage caused

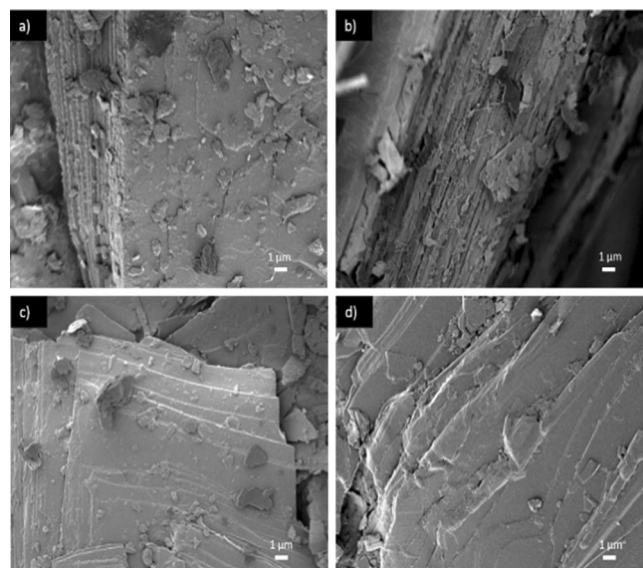


Figure 2. SEM images of a) GaS, b) GaSe, c) GaTe, and d) InSe. Scale bars: 1 μm .

during the preparation of samples, during which crystals were cut in perpendicular to the base plane.

XRD analysis was performed to confirm the phase composition. The diffractograms are displayed in Figure 3. Analysis has revealed pure gallium chalcogenides (GaS PDF# 01-071-0009; GaSe PDF# 01-080-2271; GaTe PDF# 01-071-0620) and pure InSe (PDF# 00-034-1431). No other phases, including oxides, were detected. The sharp profile of the reflections indicates very good crystallinity and strong preferential orientation due to the layered structure. The (00l) preferential orientation is observed for layered chalcogenides with hexagonal symmetry

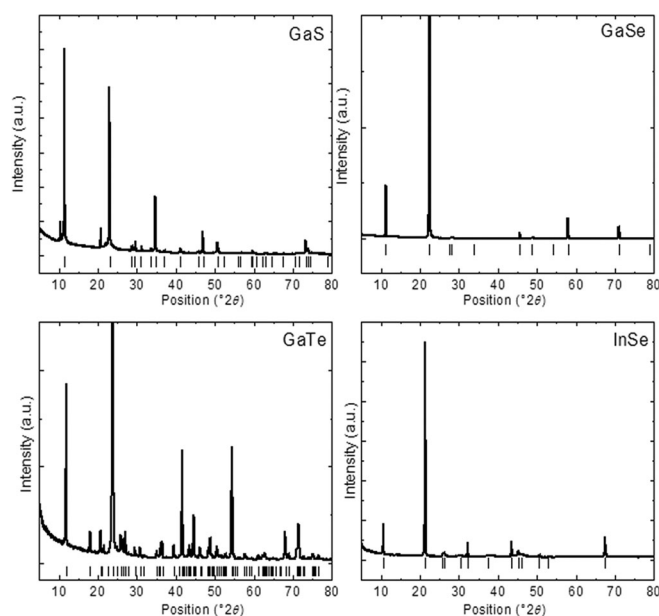


Figure 3. Diffractograms of GaS, GaSe, GaTe, and InSe. Small lines at the bottom of the spectra represent reference data taken from the PDF database.

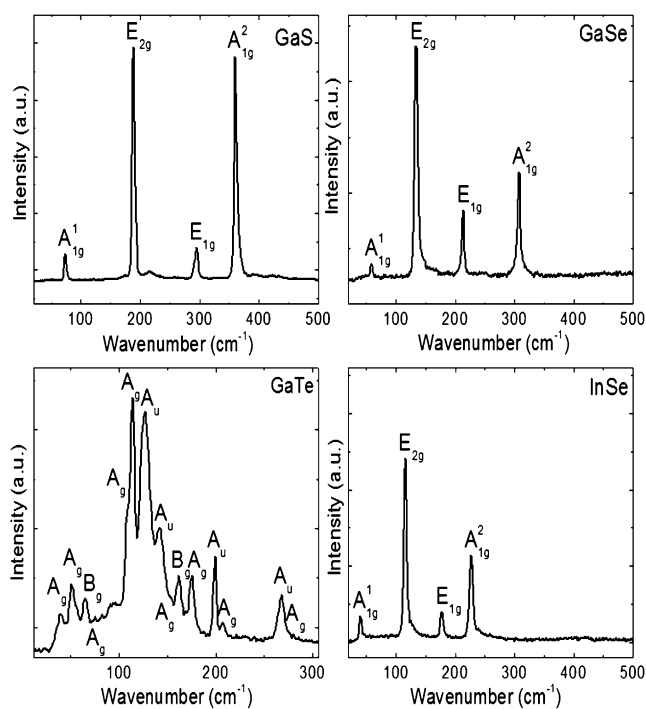


Figure 4. Raman spectra of GaS, GaSe, GaTe, and InSe.

(GaS, GaSe, and InSe), whereas for monoclinic GaTe preferential orientation in the ($h00$) direction is observed. These results are in good agreement with the morphology observed by SEM and other analytical methods (see below).

Raman spectroscopy was then used to obtain further structural information about the prepared chalcogenides (Figure 4). For GaS and InSe, which have D_{6h}^4 symmetry, and GaSe with D_{3h} symmetry (slightly different layer stacking), several vibrational modes are visible.^[28–30] These vibration modes represent both intra- (E_{2g} , E_{1g}) and interlayer (A_{1g}^1 , A_{2g}^2) interactions and are in good agreement with the literature.^[28–30] GaTe has a richer Raman spectrum because of its less symmetrical point group $B2m$. The results are nevertheless still in good agreement with the literature and indicate the successful synthesis of bulk GaTe crystals.^[31] Together with the Raman-active phonon modes (several A_g , A_u , B_g , and B_u modes), three optically active A_u modes can be seen also at 130, 143, and 200 cm^{-1} .

Photoluminescence spectra were measured by using a $\lambda = 532$ nm laser to showcase the band structure of prepared chalcogenides. GaSe shows a strong band at about 2.01 eV ($\lambda = 618$ nm), which is in an excellent agreement with previous reports on bulk GaSe crystals.^[18] Similarly, GaTe exhibits photoluminescence with a maximum centered at $\lambda = 747$ nm (1.66 eV) and is in good agreement with reports from the literature.^[32] Finally, for the InSe bulk crystals, we obtained a maximum centered at $\lambda = 995$ nm (1.25 eV), which was also in good agreement with the literature.^[30] The increase in the full-width at half-maximum (FWHM) of the luminescence peaks for GaTe and InSe indicates increasing amount of defects, as well as the effect of temperature on photoluminescence peak broadening with band gap reduction. The reported band gap value of GaS is 3.05 eV,^[33] however, excitation at $\lambda = 532$ nm leads to only

a small peak at $\lambda = 694$ nm (1.79 eV), which indicates the presence of deep levels within the GaS band gap associated with impurities or defects in the structure, such as vacancies or interstitial atoms. The results of photoluminescence measurements with excitation at $\lambda = 532$ nm are shown in Figure 5. The photoluminescence of GaS was further measured by using a He–Cd UV laser ($\lambda = 325$ nm). The absence of a luminescence signal at 3.05 eV ($\lambda = 406$ nm) originates from the fact that this direct transition is located about 0.45 eV above the indirect transition.^[34] The broad and weak luminescence maxima at $\lambda \approx 620$ and 780 nm originate from indirect band and deep level transitions, which are typically nonradiative recombinations and are accompanied only by extremely low photoluminescence yields. Results are shown in Figure S3 in the Supporting Information.

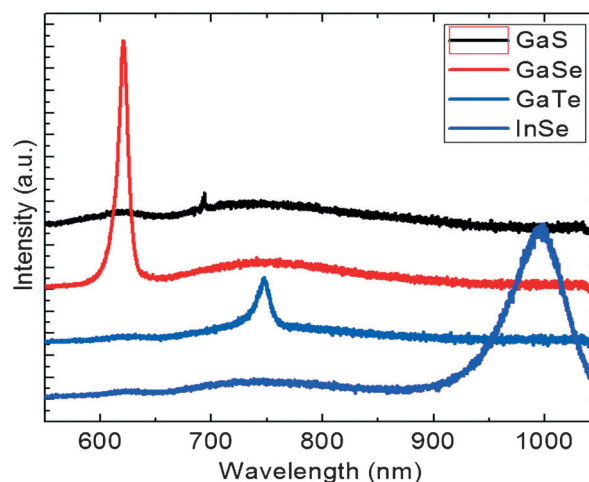


Figure 5. Photoluminescence spectra of GaS, GaSe, GaTe, and InSe measured by using a $\lambda = 532$ nm laser with 0.5 mW excitation power.

Further information about the surface chemical composition and bonding information was obtained by X-ray photoelectron spectroscopy (XPS). First, wide scan spectra were recorded (Figure S4 in the Supporting Information). The presence of oxygen and carbon in the materials is ascribed to adsorbed oxygen/moisture and adventitious carbon. From the survey spectra, the chalcogen to metal ratio was evaluated and the results are shown in Table S1 in the Supporting Information. These results show a discrepancy with the results obtained by EDS. The reasons for different ratios are due to the high surface sensitivity of the XPS method. Moreover, GaS exhibits a metal-deficient surface, whereas GaSe, GaTe, and InSe exhibit a metal-rich surface. High-resolution core-level spectra of Ga 3d and In 3d are shown in Figure 6. The deconvolution of Ga 3d revealed two pairs of peaks originating from gallium sulfide and gallium oxides. The first pair is located at about 19.5 and 19.9 eV and corresponds to the Ga–S bond, whereas the other pair is located at about 21.46 and 21.91 eV. Comparison with the literature revealed that Ga_2O_3 had a pair located at (20.4 ± 0.2) and (20.8 ± 0.2) eV.^[35] This led us to conclude that this pair does not originate from Ga_2O_3 .^[35] In the case of GaSe, only one

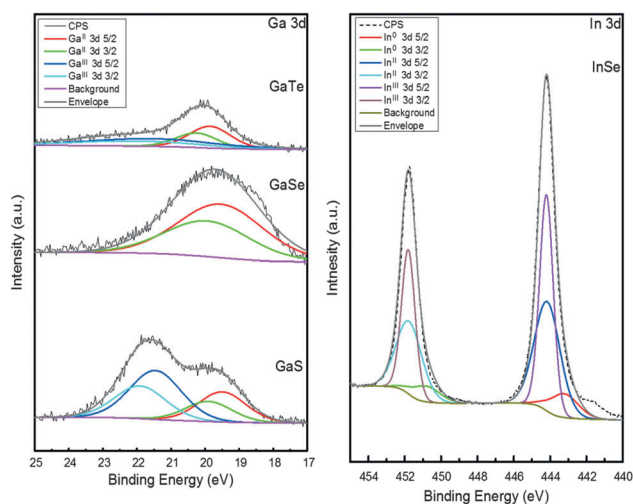


Figure 6. High-resolution X-ray photoelectron spectra of Ga 3d and In 3d of GaS, GaSe, GaTe, and InSe. C 1s peaks at about 284.5 eV are used as a calibration reference.

pair of peaks at about 19.54 and 19.94 eV is observed and attributed to the Ga–Se bond. One distinct peak of GaTe is found at about 19.8 and 20.2 eV and attributed to the Ga–Te bond. The other pair present in the spectrum originates from Ga₂O₃ located at about 20.6 and 21.05 eV, respectively. The presence of gallium oxide is due to the surface hydrolysis of chalcogenide and its subsequent oxidation in air. Furthermore, two In 3d pairs with spin-orbit split doublets at 444.16 and 451.76 eV and 444.20 and 451.80 eV ($\Delta E = 7.6$ eV), originating from In–Se and In–O, respectively, were obtained after deconvolution.^[10] Also, some indium in the indium(0) oxidation state was detected. This may indicate partial surface disproportionation of In²⁺ in InSe into In³⁺ and In⁰.

The potential window at which individual materials may operate is always limited due to their inherent electrochemistry or solvent-related electrochemical reactions.^[36] At present, fundamental electrochemical studies of A^{III}B^{VI} layered chalcogenides and their inherent electrochemistry are not adequate.^[12] To further investigate the nature of processes that occur when external voltage is applied, we conducted cyclic voltammetry (CV) in both anodic and cathodic scan directions over the range of -1.8 to $+1.8$ V in a 0.05 M solution of phosphate-buffered saline (PBS; pH 7.2). Three consecutive scans were performed to reveal the electrochemistry of the material's surface. Figure 7 and Figure S5 in the Supporting Information display the cyclic voltammograms of GaS, GaSe, GaTe, and InSe in both anodic and cathodic scan directions. All gallium chalcogenides show an inconspicuous peak at about -0.6 V (Figure S5 in the Supporting Information). From measurements of Ga₂O₃ in PBS shown in Figure S6 in the Supporting Information, we can conclude that this process is likely to be related to the reduction of Ga₂O₃ on the surface of Ga chalcogenides. This is also very well supported by the fact that this reduction peak only appears after cycling to anodic potentials, at which a small oxidation peak at about $+1.3$ V can be seen; this may lead to oxidation of the material's surface to moieties such as

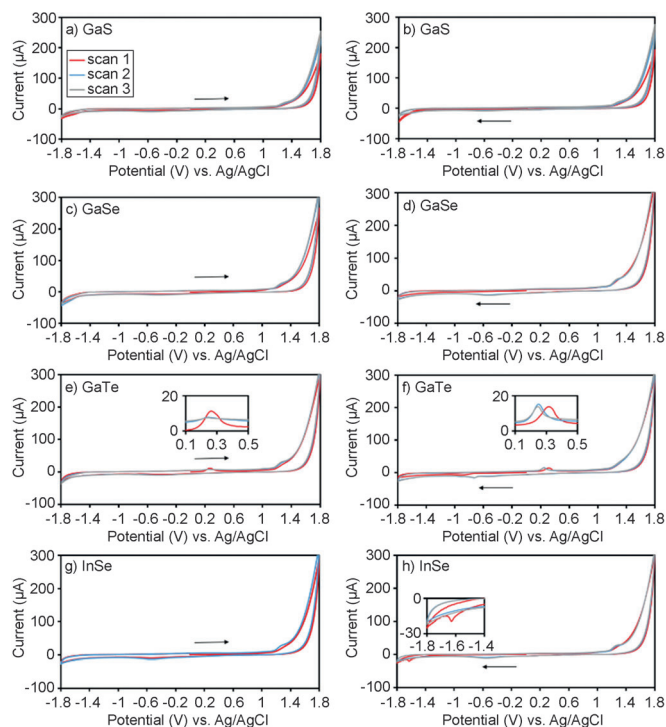


Figure 7. Cyclic voltammograms of the a) anodic and b) cathodic scans, GaSe during the c) anodic and d) cathodic scans, GaTe during the e) anodic and f) cathodic scans, and InSe during the g) anodic and h) cathodic scans. Arrows represent the scan direction. Conditions: 0.05 M PBS (pH 7.2) as a supporting electrolyte; scan rate, 100 mV s⁻¹.

Ga₂O₃ (Figure S5 in the Supporting Information). CV data also indicate that repetitive cycling makes the surface more electrochemically active, as documented by the increase in current during subsequent scans. In addition, GaTe shows an oxidation peak at about $+0.3$ V, which shifts to slightly lower potentials in subsequent scans in both anodic and cathodic directions. A very slight peak at about -1.0 V, which is much more pronounced in the cathodic scan direction, can also be seen in Figure S5 in the Supporting Information. Because no similar peaks were detected in the CV curves of GaS and GaSe, it is unlikely that these peaks originate from Ga compounds (also in good agreement with XPS, for which no or very little Ga oxides were detected), so we suggest that these peaks are related to redox processes of Te. Finally, InSe exhibits a reduction peak at about -1.6 V during cathodic scanning. The absence of this peak during anodic scanning suggests that anodic scanning deactivates this reducible moiety at the material's surface. By comparison with data obtained from the measurement of In₂O₃ (Figure S6 in the Supporting Information), we conclude that this process is related to the reduction of In₂O₃, leading to the formation of insoluble products that inhibit the further course of this reaction. Also, an inconspicuous peak located at about $+1.3$ V emerges during the anodic scan. Interestingly, this oxidation process inhibits the reduction of In₂O₃ previously described, but gives rise to a new reduction peak located at about -0.6 V in subsequent scans. Unfortunately, due to a lack

of data on this topic in the literature, precise determination of these redox processes was not possible.

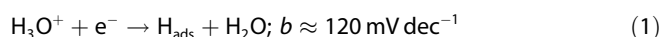
Previous research into layered materials has revealed their excellent performance in electrocatalysis. For example, 2D MoS₂ and WS₂ are very efficient for the HER.^[37–40] Some papers reported A^{III}B^{VI} layered chalcogenides as excellent HER catalysts. GaS nanosheets obtained by liquid exfoliation show much better HER performance with smaller nanosheets than that with larger nanosheets, which suggests that the catalytic site of GaS for the HER is located at the edge of the sheets.^[11] Other work has investigated the performance of bulk GaSe towards the oxygen evolution reaction (OER), oxygen reduction reaction (ORR), and the HER, revealing that electrochemical pretreatment could enhance the HER catalytic activity.^[12] Currently, there is a lack of knowledge about the catalytic activity of A^{III}B^{VI} layered chalcogenides, which makes them attractive for further research.

The HER performance of bulk GaS, GaSe, GaTe, and InSe is shown in Figure 8 and Figure S7 in the Supporting Information. It is clear that all four materials show poorer HER performances than bare GC. It has been reported that active sites for the HER are at the edge of materials with X–M–M–X structures.^[11,12,41] Therefore, the reason for the poor HER performance is mainly due to low conductivity and less active sites being present in the bulk state. Although these materials exhibit low catalytic activity towards the HER, it is of interest to compare the HER performance in detail. As shown in Figure 8a, the best performing electrocatalyst for the HER is GaSe followed by GaS and GaTe. XPS analysis revealed no gallium oxide on the surface of GaSe, which may substantially contribute to the better HER performance.^[12] Furthermore, InSe shows a peak at about –1.0 V versus RHE during the initial scan, which disappears in subsequent scans. This peak originates from the inherent electrochemistry of InSe and was discussed above. The shift in potential can be caused by different pH values compared with inherent electrochemistry measurements. Subsequent scans were also performed that revealed, for gallium chalcogenides, the overpotential became slightly lower, which indicated activation of the material's surface (Fig-

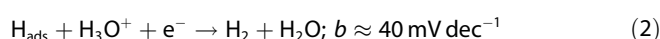
ure S7 in the Supporting Information). On the contrary, InSe shows the opposite trend. This is likely to be caused by insoluble products formed on the surface of InSe during electrochemical reduction observed in the first HER cycle.

Another way to measure the catalytic activity of HER catalysts is the Tafel slope value. The results of Tafel slope analysis are shown in Figure 8d. The Tafel slope values can be used to determine the rate-limiting step for the HER. Generally, the rate-limiting steps are those given by Equations (1)–(3):^[38,42,43]

1. Adsorption step (Volmer):



2. Desorption step (Heyrovsky):



3. Desorption step (Tafel):



The values of the Tafel slopes indicate that the Volmer adsorption step [Eq. (1)] is the rate-limiting step for all of the materials. Similarly to overpotential, the Tafel slope value decreases for GaS, GaSe, and GaTe with subsequent scans; this indicates their activation. For InSe, the Tafel slope value increases gradually, in good agreement with previous discussions.

Conclusion

We have successfully prepared single-phase A^{III}B^{VI} layered chalcogenides (GaS, GaSe, GaTe, and InSe). The synthesized materials were characterized in detail by means of XRD, XPS, EDS, Raman spectroscopy, and photoluminescence spectroscopy. The layered structure is clearly visible in SEM images. All of these materials exhibit negligible inherent electrochemistry; this is related to surface oxidation originating from either natural oxidation or anodic potential sweeping. Energy-related research into A^{III}B^{VI} layered chalcogenides towards the HER shows their relatively low HER performance due to lower conductivity and fewer active sites in the bulk state. Further HER investigation after exfoliation has to be performed in the future. We believe that these findings of their electrochemical properties will contribute to finding possible applications in the future.

Experimental Section

Materials

Gallium (99.999%), indium (99.999%), and sulfur (99.999%) were obtained from STREAM (Germany). Selenium (99.999%) and tellurium (99.999%) were obtained from Chempur (Germany). Sulfuric acid, potassium chloride, potassium phosphate dibasic, sodium chloride, and sodium phosphate monobasic were purchased from Sigma–Aldrich, Singapore. GC electrodes, Ag/AgCl reference electrodes, and Pt working electrodes were purchased from CH Instru-

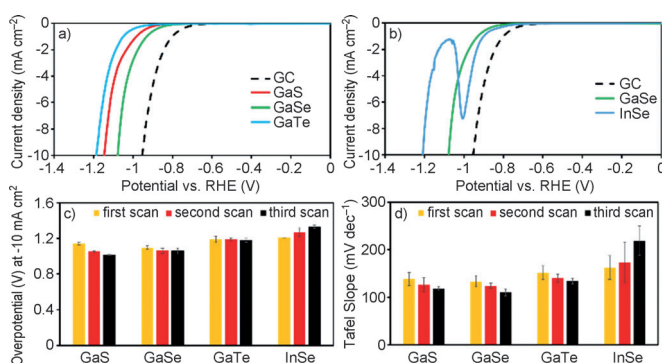


Figure 8. a) and b) Polarization curves for the HER on GaS, GaSe, GaTe, and InSe. GC = glassy carbon, RHE = reversible hydrogen electrode. c) Overpotential of three consecutive scans at a current density of –10 mA cm⁻². d) Tafel slope values of three consecutive scans. Conditions: scan rate of 2 mV s⁻¹, 0.5 M H₂SO₄ as the electrolyte.

ment, USA. Deionized water with an electrical resistivity of 18.4 MΩ cm was used to prepare suspensions and electrolytes.

Apparatus

SEM was performed by using a JEOL 7600F field-emission scanning electron microscope (JEOL, Japan), at a voltage of 2 kV. EDS data were recorded at an accelerating voltage of 15 kV. XPS measurements were carried out by utilizing a Mg_{Kα} source (SPECS, Germany) at 1253 eV, as well as a Phibos 100 spectrometer. Wide-scan and high-resolution spectra of Ga 3d, In 3d, S 2p, Se 3d, C 1s, and O 1s were obtained to analyze the surface composition and metal-to-chalcogen ratio of the materials. The 284.5 eV peak of C 1s was used for calibration. Powder XRD data were collected at room temperature with a Bruker D8 Discoverer powder diffractometer with parafocusing Bragg–Brentano geometry by using Cu_{Kα} radiation ($\lambda = 0.15418$ nm, $U = 40$ kV, $I = 40$ mA). Data were scanned with an ultrafast detector (Lynxeye XE) over the angular range $2\theta = 10\text{--}80^\circ$ with a step size of 0.02° (2θ). Data evaluation was performed in the software package Eva. An inVia Raman microscope (Renishaw, England) with a charge-coupled device (CCD) detector was used for Raman spectroscopy in back-scattering geometry. A Nd-YAG laser ($\lambda = 532$ nm, 50 mW) with a 50× magnification objective was used for measurements. Instrument calibration was performed with a silicon reference that gave a peak center at 520 cm^{-1} and a resolution of less than 1 cm^{-1} . To avoid radiation damage, the laser power output used for these measurements was kept at 5 mW. The micro-photoluminescence measurements were performed by using a Nd-YAG laser ($\lambda = 532$ nm, 50 mW) with a 50× magnification objective and $\lambda = 325$ nm He–Cd laser (22 mW) with a 40× magnification UV objective. For measurements with Nd-YAG and He–Cd lasers, laser powers of 0.5 and 2.2 mW, respectively, were used. Characterization by AFM was performed on a NT-MDT Ntegra spectrometer from NT-MDT in tapping mode. The measurements were performed on freshly cleaved basal planes. Edge planes were prepared for measurements by cutting and polishing crystals perpendicularly to the basal plane. The electrochemical measurements were conducted by using a μ Autolab III electrochemical analyzer (Eco Chemie, The Netherlands) with the NOVA version 1.8 software.

Syntheses of GaS, GaSe, GaTe, and InSe

Stoichiometric amounts of metal and chalcogen corresponding to 10 g of synthesized material were placed in a quartz glass ampoule with inner dimensions of 20 × 140 mm. The ampoule was evacuated with a pressure below 2×10^{-3} Pa and melt sealed by using an oxygen–hydrogen torch. For the synthesis of layered chalcogenides, in all experiments, a heating rate of 5°C min^{-1} and a cooling rate 1°C min^{-1} with a dwell-on temperature for 60 min were used. The synthesis of GaSe was performed at 960°C , GaTe at 860°C , and InSe at 700°C . All syntheses were performed in a muffle furnace. For the synthesis of GaS, a quartz ampoule 25 × 250 mm size was used; this was placed in a tube furnace. The part containing gallium was heated on 980°C , whereas the second part of ampoule was kept at 650°C to avoid bursting of the ampoule due to a high pressure of sulfur. The heating profile was similar to that used for other chalcogenides.

Electrochemical procedures

Suspensions (1 mg mL^{-1}) of GaS, GaSe, GaTe, and InSe were prepared by using deionized water, followed by sonication for 1 h to obtain homogeneous suspensions. An aliquot (4 μL) of the suspen-

sion was drop-casted on the GC surface, and GC could be renewed by polishing with $0.05\text{ }\mu\text{m}$ alumina particles on a polishing pad after each measurement. Deionized water was evaporated at room temperature to give randomly distributed materials. CV and linear sweep voltammetry (LSV) measurements were conducted by using a three-electrode system: modified GC, Pt, and Ag/AgCl as working, counter, and reference electrodes. PBS (50 mm, pH 7.2) was used as a background electrolyte for CV measurements at a scan rate of 100 mV S^{-1} , whereas 0.5 M sulfuric acid was utilized as an electrolyte for LSV experiments at a scan rate of 2 mV S^{-1} .

Acknowledgements

M.P. acknowledges a Tier 2 grant (MOE2013-T2-1-056; ARC 35/13) from the Ministry of Education, Singapore. Z.S. and J.L. were supported by the Czech Science Foundation (GACR no. 15-07912S) and Specific University Research Fund (MSMT no. 20-SVV/2016).

Keywords: chalcogens · electrochemistry · heterogeneous catalysis · hydrogen evolution reaction · layered compounds

- [1] a) V. Nicolosi, M. Chhowalla, M. G. Kanatzidis, M. S. Strano, J. N. Coleman, *Science* **2013**, *340*, 1226419; b) X. Chia, A. Y. S. Eng, A. Ambrosi, S. M. Tan, M. Pumera, *Chem. Rev.* **2015**, *115*, 11941; c) J. Zhou, *Appl. Mater. Today* **2016**, *2*, 24; d) M. Pumera, Z. Sofer, A. Ambrosi, *J. Mater. Chem. A* **2014**, *2*, 8981; e) Z. He, W. Que, *Appl. Mater. Today* **2016**, *3*, 23.
- [2] a) A. Splendiani, L. Sun, Y. Zhang, T. Li, J. Kim, C.-Y. Chim, G. Galli, F. Wang, *Nano Lett.* **2010**, *10*, 1271–1275; b) S. Li, S. Wang, D.-M. Tang, W. Zhao, H. Xu, L. Chu, Y. Bando, D. Golberg, G. Eda, *Appl. Mater. Today* **2015**, *1*, 60.
- [3] K. He, C. Poole, K. F. Mak, J. Shan, *Nano Lett.* **2013**, *13*, 2931–2936.
- [4] X. Huang, Z. Zeng, H. Zhang, *Chem. Soc. Rev.* **2013**, *42*, 1934–1946.
- [5] A. Kumar, P. Ahluwalia, *Eur. Phys. J. B* **2012**, *85*, 1–7.
- [6] Z. Yin, H. Li, H. Li, L. Jiang, Y. Shi, Y. Sun, G. Lu, Q. Zhang, X. Chen, H. Zhang, *ACS Nano* **2012**, *6*, 74–80.
- [7] R. B. Jacobs-Gedrim, M. Shanmugam, N. Jain, C. A. Durcan, M. T. Murphy, T. M. Murray, R. J. Matyi, R. L. Moore, B. Yu, *ACS Nano* **2014**, *8*, 514–521.
- [8] C. De Blasi, A. Drigo, G. Micocci, A. Tepore, A. Mancini, *J. Cryst. Growth* **1989**, *94*, 455–458.
- [9] H. Peng, S. Meister, C. K. Chan, X. F. Zhang, Y. Cui, *Nano Lett.* **2007**, *7*, 199–203.
- [10] J. Lauth, F. E. Gorris, M. Samadi Khoshkoo, T. Chassé, W. Friedrich, V. Lebedeva, A. Meyer, C. Klinke, A. Kornowski, M. Scheele, *Chem. Mater.* **2016**, *28*, 1728–1736.
- [11] A. Harvey, C. Backes, Z. Gholamvand, D. Hanlon, D. McAteer, H. C. Nerl, E. McGuire, A. Seral-Ascaso, Q. M. Ramasse, N. McEvoy, *Chem. Mater.* **2015**, *27*, 3483–3493.
- [12] S. M. Tan, C. K. Chua, D. Sedmidubský, Z. Sofer, M. Pumera, *Phys. Chem. Chem. Phys.* **2016**, *18*, 1699–1711.
- [13] X. Meng, K. He, D. Su, X. Zhang, C. Sun, Y. Ren, H. H. Wang, W. Weng, L. Trahey, C. P. Canlas, *Adv. Funct. Mater.* **2014**, *24*, 5435–5442.
- [14] P. Hu, L. Wang, M. Yoon, J. Zhang, W. Feng, X. Wang, Z. Wen, J. C. Idrobo, Y. Miyamoto, D. B. Geohegan, *Nano Lett.* **2013**, *13*, 1649–1654.
- [15] S. Yang, Y. Li, X. Wang, N. Huo, J.-B. Xia, S.-S. Li, J. Li, *Nanoscale* **2014**, *6*, 2582–2587.
- [16] A. Kipperman, G. Van der Leeden, *Solid State Commun.* **1968**, *6*, 657–662.
- [17] X. Li, M.-W. Lin, A. A. Puzos, J. C. Idrobo, C. Ma, M. Chi, M. Yoon, C. M. Rouleau, I. I. Kravchenko, D. B. Geohegan, K. Xiao, *Sci. Rep.* **2014**, *4*, 5497.
- [18] P. Hu, Z. Wen, L. Wang, P. Tan, K. Xiao, *ACS Nano* **2012**, *6*, 5988–5994.
- [19] K. R. Allakhverdiev, M. Ö. Yetis, S. Özbek, T. K. Baykara, E. Y. Salayev, *Laser Phys.* **2009**, *19*, 1092–1104.
- [20] W. Shi, Y. J. Ding, N. Fernelius, K. Vodopyanov, *Opt. Lett.* **2002**, *27*, 1454–1456.

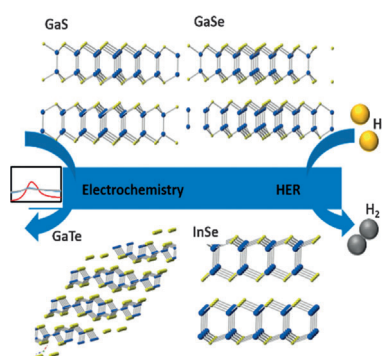
- [21] Ref. [12].
- [22] E. G. Gillan, A. R. Barron, *Chem. Mater.* **1997**, *9*, 3037–3048.
- [23] M. Abdel Rahman, A. Belal, *J. Phys. Chem. Solids* **2000**, *61*, 925–929.
- [24] J. Sánchez-Royo, A. Segura, V. Muñoz, *Phys. Status Solidi a* **1995**, *151*, 257–265.
- [25] S. Sucharitakul, N. J. Goble, U. R. Kumar, R. Sankar, Z. A. Bogorad, F.-C. Chou, Y.-T. Chen, X. P. Gao, *Nano Lett.* **2015**, *15*, 3815–3819.
- [26] W. Feng, W. Zheng, W. Cao, P. Hu, *Adv. Mater.* **2014**, *26*, 6587–6593.
- [27] S. Lei, F. Wen, B. Li, Q. Wang, Y. Huang, Y. Gong, Y. He, P. Dong, J. Bellah, A. George, *Nano Lett.* **2014**, *14*, 259–265.
- [28] N. Gasanly, A. Aydınli, H. Özkan, C. Kocabaş, *Mater. Res. Bull.* **2002**, *37*, 169–176.
- [29] N. M. Gasanly, A. Aydınli, H. Özkan, C. Kocabaş, *Solid State Commun.* **2000**, *116*, 147–151.
- [30] D. Pozo-Zamudio, S. Schwarz, J. Klein, R. Schofield, E. Chekhovich, O. Ceylan, E. Margapot, A. Dmitriev, G. Lashkarev, D. Borisenko, arXiv preprint arXiv:1506.05619 2015.
- [31] *Gallium Telluride (GaTe) Phonon Wavenumbers* (Eds.: O. Madelung, U. Rössler and M. Schulz), Springer, Berlin, Heidelberg, **1998**, pp. 1–3.
- [32] M. Yüksek, H. Ertap, A. Elmali, H. Gul Yaglioglu, G. M. Mamedov, M. Karabulut, M. K. Öztürk, *Opt. Laser Technol.* **2012**, *44*, 2178–2181.
- [33] M. Lazell, P. O'Brien, D. J. Otway, J.-H. Park, *J. Chem. Soc. Dalton Trans.* **2000**, *24*, 4479–4486.
- [34] A. Mercier, E. Mooser, J. P. Voitchovsky, *J. Lumin.* **1973**, *7*, 241–266.
- [35] H. Iwakuro, C. Tatsuyama, S. Ichimura, *Jpn. J. Appl. Phys.* **1982**, *21*, 94.
- [36] M. Z. M. Nasir, Z. Sofer, A. Ambrosi, M. Pumera, *Nanoscale* **2015**, *7*, 3126–3129.
- [37] M. A. Lukowski, A. S. Daniel, F. Meng, A. Forticaux, L. Li, S. Jin, *J. Am. Chem. Soc.* **2013**, *135*, 10274–10277.
- [38] Y. Li, H. Wang, L. Xie, Y. Liang, G. Hong, H. Dai, *J. Am. Chem. Soc.* **2011**, *133*, 7296–7299.
- [39] D. Voiry, H. Yamaguchi, J. Li, R. Silva, D. C. Alves, T. Fujita, M. Chen, T. Asefa, V. B. Shenoy, G. Eda, *Nat. Mater.* **2013**, *12*, 850–855.
- [40] J. Yang, D. Voiry, S. J. Ahn, D. Kang, A. Y. Kim, M. Chhowalla, H. S. Shin, *Angew. Chem. Int. Ed.* **2013**, *52*, 13751–13754; *Angew. Chem.* **2013**, *125*, 13996–13999.
- [41] H. Gerischer, J. Gobrecht, J. Turner, *Ber. Bunsen Ges. Phys. Chem.* **1980**, *84*, 596–601.
- [42] J. Thomas, *Trans. Faraday Soc.* **1961**, *57*, 1603–1611.
- [43] J. M. Bockris, E. Potter, *J. Electrochem. Soc.* **1952**, *99*, 169–186.

Received: September 2, 2016

Published online on ■ ■ ■, 0000

FULL PAPER

Electrochemistry

*J. Luxa, Y. Wang, Z. Sofer, M. Pumera** Layered Post-Transition-Metal
Dichalcogenides (X–M–M–X) and
Their Properties

Stacked catalysts: A^{III}B^{VI} chalcogenides are an interesting group of layered semiconductors with several attractive properties, such as tunable band gaps and the formation of solid solutions. Single-phase A^{III}B^{VI} layered chalcogenides were prepared and their inherent electrochemistry and hydrogen evolution reaction (HER) catalytic properties were explored (see figure).